Designing micro- and nanostructures for artificial urinary sphincters

Florian M. Weiss[a], Hans Deyhle[a], Gabor Kovacs[b], and Bert Müller*[a]
[a]Biomaterials Science Center, University of Basel, c/o University Hospital, 4031 Basel, Switzerland;
[b]Swiss Federal Laboratories for Materials Science and Technology, 8600 Dübendorf, Switzerland

ABSTRACT

The dielectric elastomers are functional materials that have promising potential as actuators with muscle-like mechanical properties due to their inherent compliancy and overall performance: the combination of large deformations, high energy densities and unique sensory capabilities. Consequently, such actuators should be realized to replace the currently available artificial urinary sphincters building dielectric thin film structures that work with several 10 V. The present communication describes the determination of the forces (1 – 10 N) and deformation levels (~10%) necessary for the appropriate operation of the artificial sphincter as well as the response time to master stress incontinence (reaction time less than 0.1 s). Knowing the dimensions of the presently used artificial urinary sphincters, these macroscopic parameters form the basis of the actuator design. Here, we follow the strategy to start from organic thin films maybe even monolayers, which should work with low voltages but only provide small deformations. Actuators out of 10,000 or 100,000 layers will finally provide the necessary force. The suitable choice of elastomer and electrode materials is vital for the success. As the number of incontinent patients is steadily increasing worldwide, it becomes more and more important to reveal the sphincter's function under static and stress conditions to realize artificial urinary sphincters, based on sophisticated, biologically inspired concepts to become nature analogue.

Keywords: Artificial urinary sphincter, electrically activated polymers, organic molecular beam deposition, silicone, ultra-violet light-based cross-linking

1. INTRODUCTION

Urinary incontinence is one of the largest markets for MedTech companies, which is still underdeveloped. The demographic shift to a higher percentage of elderly residents even further increases the demand for nature-analogue devices to not only handle the static situation but also to treat stress incontinence. Current commercially available implants for patients suffering from severe urinary incontinence have serious restrictions, which regularly result in atrophy and erosion a very few years after implantation [1]. Recently, cutting-edge technologies leading to first application of an efficient incontinence treatment were proposed see e.g. ref. [2]. Stress incontinence is the involuntary loss of urine during increased abdominal pressure, which occurs during coughing and physical exercises. In our society, about 30% of males at the age of 70 are incontinent, with serious implications for their quality of life [3]. The up-to-date treatment of severe incontinence involves the AMS 800™, a relatively simple, purely mechanically driven device. Its clinical success is rather limited especially because a constant pressure is acting on the urethral tissue [4]. Consequently, implants have to be removed within the first five years, although the implant system and its handling have been steadily improved during more than two decades [1, 5-7]. EAP actuators are expected to improve the current treatment, because they allow a millisecond response to the exterior stresses. Another attractive feature of electro active polymers (EAPs) is their ability to emulate biological muscles with high stiffness, large strains and inherent vibration damping. Note that an ideal dielectric elastomer has liquid-like behavior similar to that of the urethral tissue.

During the last decade the interest for smart materials that respond to external stimuli changing their shape or size has considerably increased. Beside the more conventional approaches materials including hydro-gels, dielectric elastomers, shape memory polymers, conducting polymers, carbon nanotubes and ferroelectric liquid crystalline elastomers have been investigated [8-14]. Especially EAPs became of vital interest for high-performance actuation with required compliance [15, 16]. Among the electronic EAPs especially the dielectric elastomers are smart materials that have promising potential to be used as actuators with muscle-like mechanical properties. The combination of large deformations, high energy densities and sensory capability is unique to dielectric elastomers. This family of smart polymer materials is currently drawing a significant scientific interest, since they are capable of responding to electrical stimuli, with significant changes of size and/or shape [15, 16].

bert.mueller@unibas.ch; phone +41 61 265 9660; fax +41 61 265 9699; www.bmc.unibas.ch

Electroactive Polymer Actuators and Devices (EAPAD) 2012, edited by Yoseph Bar-Cohen,
Proc. of SPIE Vol. 8340, 83400A · © 2012 SPIE · CCC code: 0277-786X/12/$18 · doi: 10.1117/12.914649

A variety of dielectric elastomer actuators demonstrates the versatile capabilities of this technology. It involves the extender (planar), uni-morph-, bi-morph-, stack-, folded-, helical-, spring roll-, push-pull-, bow-tie-, diamond-, diaphragm-, spider-, inchworm segment-, and universal muscle actuator [17-20]. The rolled actuators with a dielectric film wrapped around a pre-loaded coil spring are intensively studied [21, 22]. So far this was used for driving small walking bug robots, large human-like upper arm robots with high force capabilities [23] and acoustic filters [24].

Nowadays silicone and acrylic based polymers are used as dielectric elastomers in actuator configurations because of their proper elastic and dielectric behavior. Beside the mechanical, electrical and electro-mechanical characterization of the materials, the fabrication and operation of devices is intensively studied to determine the influence of parameters such as pre-strains or thicknesses of the elastomer film on the performance of the actuators [22, 25]. The acrylic based elastomer VHB 4910 manufactured by 3M exhibits electro-mechanical strains of up to 210%, produces pressures of up to 8 MPa and yields specific elastic energy densities of 3.4 J/g. Different silicone films reveal microseconds response times, reasonably small dissipative losses and high stability when exposed to temperature changes, humidity or ultra-violet radiation. Additionally, silicones can easily be tailored for medical application. The strain levels of silicone actuators, however, only reach values of up to 64%. Furthermore, the actuation force density of the silicone films is lower than that of acrylic ones, since the specific electric breakdown strength of 100 V/μm is a factor of two lower than the one found for pre-strained acrylic films. Acrylic actuators so far provide the highest specific electro-mechanical performance in the quasi-static actuation mode [15].

To meet the requirements with respect to reliability and contractive motion, actuator designs in stack configuration have been evaluated, which produce contraction motion and tensile force in film thickness direction when actuated [16]. Silicones and post-processed acrylic films offer the option of sheeting in stress-free condition. In this configuration the stack actuator can directly turn electric energy into mechanical work with an electrode pressure of 0.2 N/mm^2 and a contraction of up to 45% [26].

Further, the electrodes also represent an active field of research. The solutions range from structured thin metal films [27] via metal ion implantation [28] to carbon black particles in a soft polymeric matrix [29] and single wall carbon nanotubes. Optimized fabrication methods including physical vapor deposition have been applied to reach better performance resulting from low electric resistance [27].

This proceedings contribution provides first steps in preparing and characterizing nanometer-thin elastomers with compliant electrodes to be applied for nano-actuators in artificial urinary sphincters. This approach starts from organic monolayers prepared under ultra high vacuum (UHV) conditions. It will have two main impacts, namely the research on the deposition and characterization of organic thin film deposited monolayer by monolayer, and the development of the related characterization and the development of artificial muscle nanostructures, replacing the currently 10 to 50 μm-thick films by nanometer-thin films allowing multilayer device fabrication, reducing actuation voltage and increasing force.

2. GENERAL CONSTRAINTS IN URINARY SPHINCTER DESIGN

2.1 Physical description of the urethra

The *urethra compression model* [30] comprises the three empirical parameters p_W, F_R, and L_R, which allow estimating the necessary pressure p_{ex} to close the urethra for any given bladder pressure p_{ves}, sphincter length L, and sphincter radius R:

$$p_{ex} = \left(p_{ves} + p_W\right) \cdot \left(1 + \frac{2L_R}{L}\right) + \frac{F_R}{RL} \tag{1}$$

Because of the visco-elastic behavior of the human urethral tissue [31], one has to discriminate between the situations where the urethra is closed and should remain closed and the closing of the open urethra. For the two situations, Marti et al. [30] found (-870 ± 110) Pa, (0.10 ± 0.02) N, and (5.1 ± 0.3) mm as well as (-1280 ± 90) Pa, (0.06 ± 0.02) N, and (3.0 ± 0.3) mm for p_W, F_R, and L_R. Marti et al. [30] further showed that the optimal sphincter length to close the open urethra corresponds to (17.3 ± 3.8) mm in agreement with the length of the AMS 800™. This length, however, is less relevant, since the urethra is only closed after passing water. For the other situation, where the urethra should remain in closed state, the optimal length corresponds to (8.2 ± 1.6) mm.

2.2 Forces to reach continence

More complicated, however, is the optimization of the necessary forces and pressures. For sure, they depend on the bladder pressure as given in Eq. (1). If the applied sphincter pressures are too high, one observes tissue damages mentioned above. If the pressures are too low, the patient looses urine and needs diapers. An adaptation of the sphincter pressure similar to the one observed in the healthy state is highly desirable but not realized within the commercially available devices. For a bladder pressure of 4 kPa one needs an external pressure of about 6 kPa, for a typical Valsalva manoeuvre of 5.8 kPa about 9 kPa and for coughing with 8.7 kPa about 13.5 kPa. Therefore, one can conclude that the artificial sphincter should generate a pressure of maximal 13.5 kPa or a force of maximal 1.3 N. If one concentrates on the static situation with 4 kPa and allows stress incontinence, the necessary pressure is 6 kPa. The necessary force corresponds to 0.6 N.

2.3 Strain required to switch from close to open and vice versa

The anatomy of the human urethra significantly differs between male and female. Furthermore, it is patient specific. Therefore, the present suppliers provide devices, which account for the different diameters of the urethras. For generic estimates, however, one can assume an inner diameter of 5 mm and a wall thickness of 5 mm. Assuming cross-section conservation one can close the urethra reducing the outer diameter from 15 to 14 mm, i.e. by about 7%.

Simple in vitro experiments, however, demonstrate that it is not necessary that the urethra is fully open to pass water. An urethra lumen constricted to 1 mm allows to empty the bladder within short periods of time. Therefore, strains more than an order of magnitude less than 7% could be enough for a successful development of an artificial urinary sphincter.

2.4 Materials selection for dielectric EAPs

The Maxwell pressure p can be written as:

$$p = \varepsilon_r \varepsilon_0 \left(\frac{U}{z} \right)^2 \tag{2}$$

with the applied voltage U, the layer thickness of the elastomer z and the relative dielectric constants of the elastomer and of the vacuum ε_r and ε_0, respectively. Equation (2) can be used to determine the electric field, which is required for the sphincter. For example, one may consider the silicone rubber ELASTOSIL® RT 601 A/B (Wacker Chemie AG, Stuttgart, Germany. The breakdown field is 23 kV/mm. This value is significantly higher than the electric field needed for a bladder pressure of 4 kPa, which corresponds to about 16 kV/mm. The limiting factor might be, however, the contraction path. Here, the effective Young's modulus, for the silicone rubber mentioned above it corresponds to 0.5 MPa [32], has to be incorporated into Equation (2). The estimations show that for the silicone rubber mentioned a strain of 1.2% can be reached without any problem, but values above 2.5% are problematic because of the breakdown voltage.

These rough estimates demonstrate the feasibility of the approach but have to be taken with care. For improved estimations, which include multilayer designs and the stiffening caused by the electrodes, the actual material properties of the elastomer, i.e. the relative dielectric constant, the Young's modulus, and the breakdown voltage, have to be known.

3. LAYERED DESIGN OF THE ACTUATOR FOR AN URINARY SPHINCTER

3.1 General

The present study aims at the realization of a multilayer actuator consisting of nanometer-thin elastomer deposits, prepared by physical evaporation under ultra-high vacuum (UHV) conditions. Such an approach results in further demands to the elastomer, including UHV compatibility. Here we concentrate on silicones, since this class of elastomers does not only exhibit fast response times [33], an adequate elastic behavior and a low dissipation factor [25] but also the necessary biocompatibility.

3.2 Cross-linking of the selected elastomers

Since only the monomer/oligomer units of polymers can be evaporated (cp. vapor pressures), the deposited monomers/oligomers have to be cross-linked subsequently. Although different approaches can be adapted, the

application of ultra-violet light (UV) is straightforward. The successful application of UV radiation for cross-linking implies the presence of functional groups to be radicalized. Vinyl and acryl groups possess these features. Table 1 lists vinyl- or phenyl-containing polydimethylsiloxane (PDMS) commercially available from ABCR GmbH & Co. KG (Karlsruhe, Germany). These oligomers contain functional groups with given percentages, located either at the end, as co-polymer or a combination of both.

Table 1. Selected PDMS oligomers commercially available from ABCR GmbH & Co. KG (Karlsruhe, Germany).

Product	Comment to functional groups	Viscosity [cSt]
AB 109387	Diphenyl (3-3.5%) vinyl terminated	500
AB 112089	Diphenyl (3-3.5%) vinyl terminated	10'000
AB 116641	Diphenyl (4-6%) vinyl terminated	500
AB 111905	Diphenyl (4-6%) vinyl terminated	10'000
AB 116647	Vinyl co-poly. (7-8 mol%) trimethyl terminated	800 - 1'200
AB 130289	Diphpenyl (35-40%) vinyl (3-5%)	250 - 350
AB 109409	PDMS gum, Diphenyl (6-7%) vinyl (0.1-0.2mol%)	
AB 100977	Vinyl phenyl terminated	

To obtain an optimized wavelength to cross-link the PDMS oligomers UV-VIS measurements were performed with an Agilent 8453 Spectrophotometer and processed with UV-Visible Chemstation (Rev.B.01.01[21]; Agilent Technologies, Basel, Switzerland). For this purpose, the oligomers were dissolved in cyclohexane (HPLC grade, Fisher Scientific, Wohlen, Switzerland). The units are arbitrary, since the molecular weight was unknown for several products. The investigation started with an estimated concentration of about 10^{-5} mol/L. Thereafter, the concentration was further diluted (see Figure 1).

The absorption measurements reveal a prominent peak at a wavelength of 210 nm for all oligomers at starting concentration. The smaller concentrations prepared by dilution give rise to peak shifts towards significantly shorter wavelengths of about 196 nm. Cooperative/structural effects can be used to explain this peak shift. A second absorption band present around a wavelength of 260 nm is more distinct in the data of the phenyl containing oligomers. As the solution is diluted this absorption band decreases or even vanishes.

The absorption measurement of the selected PDMS illustrates that the wavelength for UV-radiation-based cross-linking should be set to 197 nm to reach an efficient cross-linking rate. This conclusion might also rationalize the observation that the cross-linking takes place within very short periods of time for thicker films, whereas below certain thicknesses the cross-linking is only partially achieved or even absent because the UV-light passes through the microstructure without significant energy transfer.

3.3 Thermal gravimetric analysis of the selected elastomers

In order to determine the boiling point of the PDMS oligomers, thermal gravimetric analysis was carried out using the TGA/SDTA851e system (Mettler Toledo, Greifensee, Switzerland) with the STARe Software (Version 9.30 Mettler-Toledo AG1993-2009). The data were acquired with a heating rate of 10 K/min in nitrogen atmosphere. The curves displayed in Figure 2 do not allow for the determination of the boiling point. They gradually change from 200 to 300 °C, a range where the boiling point is expected. This behavior is attributed to the broad distribution of the polymer weight after cross-linking. Differential scanning calorimetry measurements are planned to identify a boiling point range with necessary precision. The weight loss observable between 450 and 550 °C is associated with the decomposition of the oligomers.

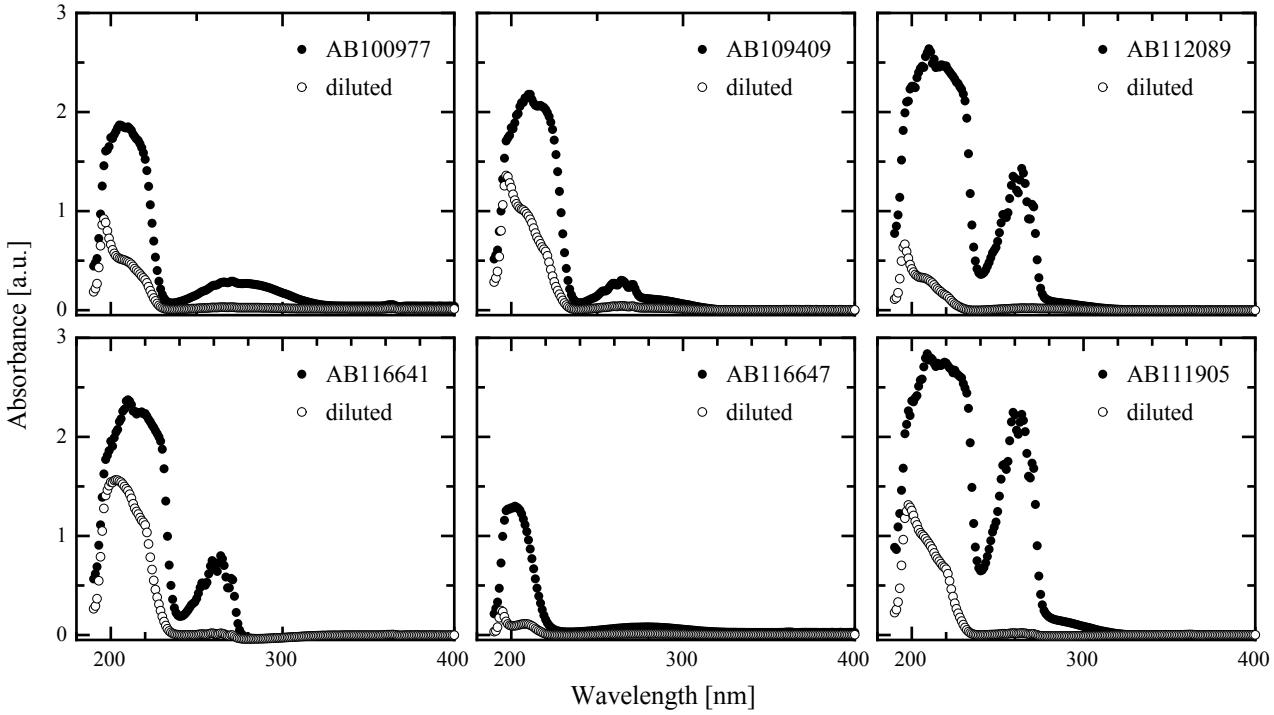

Figure 1. The diagrams show the absorption measurements of the PDMS oligomers (cp. Table 1).

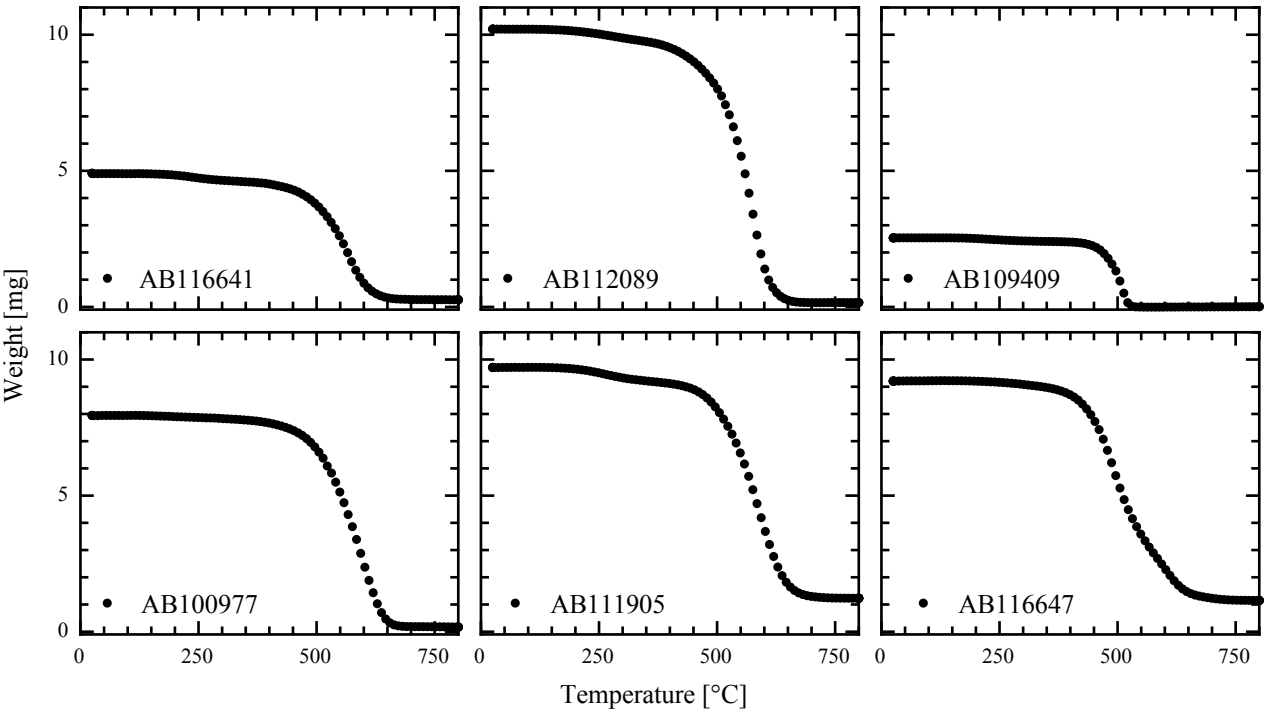

Figure 2. The diagrams show the thermal gravimetric analysis of the PDMS oligomers (cp. Table 1).

3.4 Detection scheme

In order to observe the deformation of the (single-layer) actuator one can simply measure the thickness changes as the function of the applied voltage (see upper part of Figure 3). As an alternative, one can deposit the actuator onto a micro-cantilever and determine the bending of the cantilever as the function of the applied voltage as indicated in the lower part of Figure 3. Here we propose to use either single-crystalline 30 µm-thin silicon or amorphous 25 µm-thin APTIV™ polyetheretherketone films (Series 2000) commercially available by Wafer World Inc. (West Palm Beach, FL, USA) and Victrex Europa GmbH (Hofheim, Germany), respectively.

Before the elastomer can be deposited and cross-linked the first electrode has to be built up. In similar manner, the second electrode has to be formed after elastomer deposition.

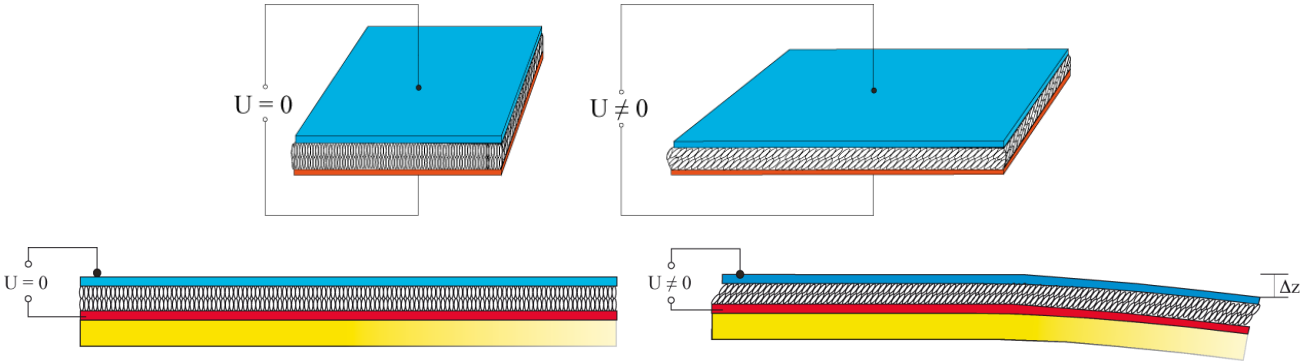

Figure 3. The application of a voltage reduces the thickness of the symmetric actuator (upper part). The attachment of the actuator onto a micro-cantilever and the subsequent application of a voltage force the asymmetric microstructure to bend. The bending radius can be precisely measured by means of a reflected laser beam. Small changes in the bending radius lead to a related displacement on the position-sensitive detector.

3.5 Choice of the top electrode

The EAP-structure was deposited on a rectangular part of a 30 µm-thin Si(001) 4-inch wafer [34]. First, a 50 nm-thin metal contact using Au, Au/Cr or Ti was grown (Nordiko Ltd. NS 2550, Hampshire, UK, and Pfeiffer ONF 010, Asslar, Germany). Subsequently, the micrometer-thick silicone film was placed using spin coating (Laurell WS-400A 6NPP, North Wales, PA, USA). On top of the silicone, the other contact was built again by means of physical vapor deposition. The morphologies of these films were observed using optical microscopy (Leica DMRM, Heerbrugg, Switzerland) and atomic force microscopy (Nanosurf Mobile S, Liestal, Switzerland).

The metal films deposited onto the silicone film with sputtering or thermal techniques did not result in flat structures but exhibited a characteristic regular ripple pattern (see Figure 4, example Ti). The periodicity of the pattern formed depends on the contact metal choice and thickness. The width of the stripes l agrees to the predictions [35]:

$$l = 4.36 \cdot t \cdot \left(\frac{E_m (1 - \nu_p^2)}{E_p (1 - \nu_m^2)} \right)^{\frac{1}{3}} \tag{3}$$

where t denotes the film thickness and E and ν correspond to the Young's modulus and the Poission's ratio of the polymer and metal, respectively. Optical micrographs, as represented in Figure 4, were Fourier transformed to extract the periodicity with high precision. A thickness of 50 nm Au on Elastosil RT 601 (Wacker, Munich, Germany) leads to microstructures with a periodicity of 2.5 µm. Using the same elastomer but 50 nm-thin Ti or Cr, one finds periodicities of 4.0 µm and 6.0 µm, respectively.

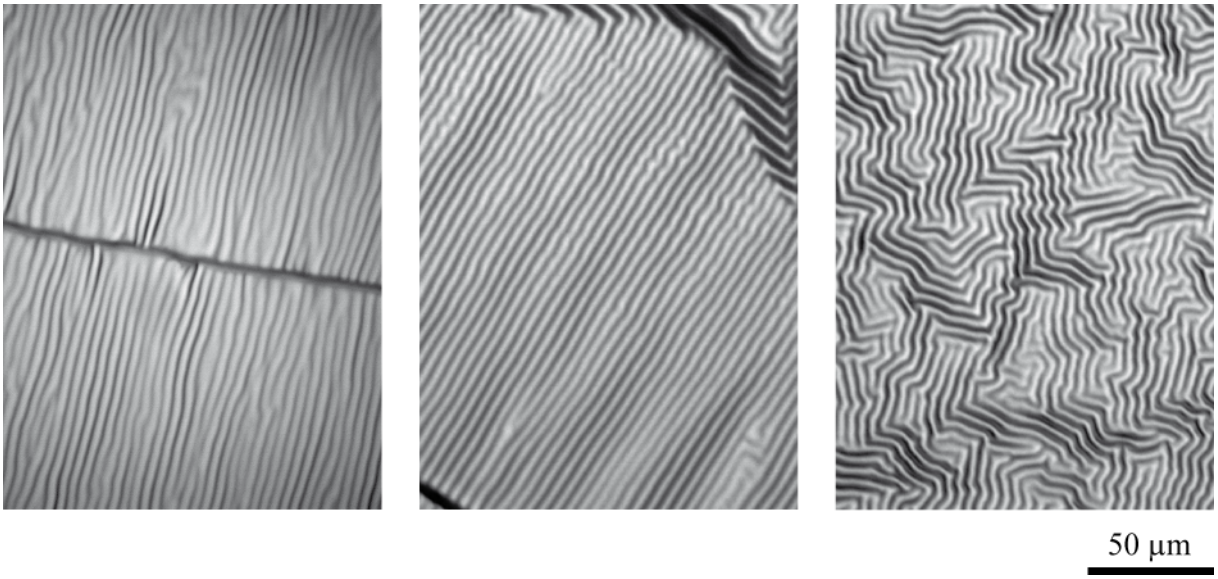

Figure 4. The ripples are arranged perpendicular to grooves (image on the left and the center). In a certain distance to the groove (cp. central image) the ripples change their direction. Far away from defects the ripples show no preferential orientation (image on the right). The periodicity, however, remains constant.

The Ti/elastomer microstructures on the silicon substrate often contain straight grooves [34]. The left and central images of Figure 4 show that the ripples are aligned perpendicular these grooves, as to other defects [32]. At a distance of about 200 µm the orientation of the ripples changes (see central image of Figure 4). Far from grooves, the stripes do not show any preferential orientation (see Figure 4, right image). The periodicity of the stripes, which exhibit height modulations of up to 10% of the silicone thickness, however, remains constant. The grooves are much deeper (30% of the film thickness).

In order to avoid the ripple formation, the electrode material has to possess special elastic and thermal properties, which is the exception. As an alternative, one may use an evaporation source, which does not increase the temperature of the substrate surface.

If it becomes possible to align the ripples (corrugations), for example intentionally introducing defects, one may even take advantages from this phenomenon [36] as proposed in similar manner more recently [37].

3.6 Formation of multilayer structures

Multilayer structures are desirable to obtain the suitable values for strain and force of artificial muscles while keeping the applied voltage in physiologically relevant ranges for the medical implant. Physical vapor deposition allows inclined incidence of the molecular beam, as shown in Figure 5. Alternating deposition from the left (red-colored arrow) and from the right (blue-colored arrow) permits the formation of joint contacts of the individual layers even with nanometer thickness. Such a procedure requires either two evaporation sources for the electrode material or substrate rotation. In between the deposition of the electrodes, the elastomer layer has to be formed without coating of the two electrical contacts. The installation of movable masks is another option.

It should be noted that the electrodes generally stiffen the multilayer structure considerably. Therefore, alternatives to the classical metal deposits have to be evaluated. The application of a thin layer of single-walled carbon nano-tubes (P3-SWCNT) as electrode material for reliable operation with fail-safe properties was proposed [38]. The high length-to-diameter aspect ratio and high electrical conductivity with self-clearing effect make carbon nano-tubes suitable as compliant electrode materials. It can self-clear around defects, electrically isolating those defects and leaving the rest of the active area functional. The self-clearing of SWNT results from the instability (degradation) of SWNT under arcing condition, owing to their highly curved tube structure. Furthermore, arcing takes place during dielectric discharging (breakdown) between the electrodes propagating radially from the pinpoint until the cleared area becomes too large to sustain the arcing. Printing of CNT has been evaluated as the appropriate application method in order to obtain the nanometer thickness.

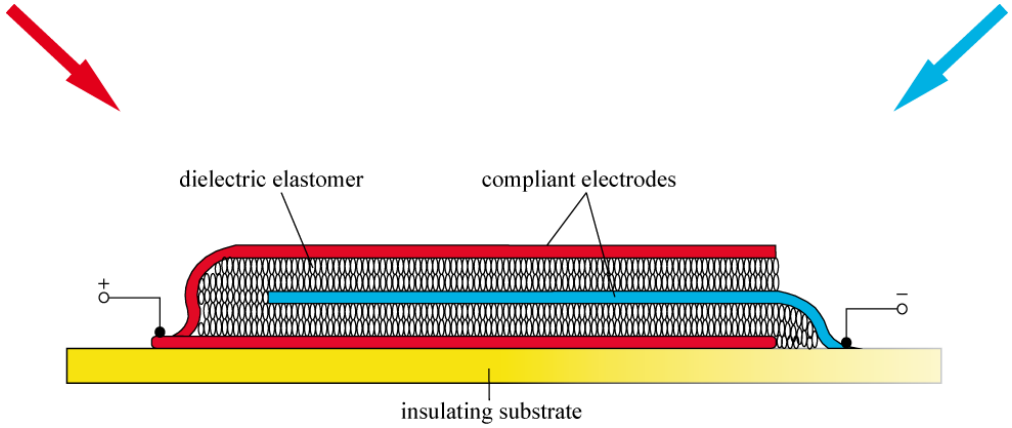

Figure 5. The ripples are arranged perpendicular to grooves (image on the left and the center). In a certain distance to the groove (cp. central image) the ripples change their direction. Far away from defects the ripples show no preferential orientation (image on the right). The periodicity, however, remains constant.

4. DISCUSSION

The appropriate treatment of severe urinary incontinence is still an unsolved clinical problem. Recently, the company Myopowers SA (Lausanne, Switzerland) introduced the piano effect into artificial sphincters that allows tissue regeneration by switching between two or more sphincter modules. This concept is well compatible with the coupled oscillators for EAP-structures for example presented by M. O'Brien and coworkers [39].

Dielectric EAP nano- and microstructures are well suited to treat stress incontinence, as the response time is in the millisecond range. The "need for speed" has been impressively demonstrated [40]. The electrodes fabricated by low-energy ion implantation provide high Q-factors. Electrical field strengths of 40 V/µm are reasonable values.

Before any EAP device to treat urinary incontinence can be prototyped, a variety of serious problems has to be mastered. Each progress in solving the tasks will broaden the fundamentals in organic thin film deposition and characterization, the knowledge on mechanical properties of organic thin films and compliant contacts and finally in implant design.

ACKNOWLEDGEMENT

We gratefully acknowledge the financial support of the Swiss National Science Foundation within project 200021-135496.

REFERENCES

[1] A. Mourtzinos, J. J. Smith, and D. M. Barrett, "Treatments for male urinary incontinence: A review," AUA Update Series, 24, 121-132 (2005).

[2] B. Müller, H. Deyhle, S. Mushkolaj et al., "The challenges in artificial muscle research to treat incontinence," Swiss Medical Weekly, 139, 591-595 (2009).

[3] H. Heidler, "Spezielle Ursachen der Harninkontinenz beim Mann," J. Urol. Urogynäkologie, 11(1), 17-18 (2004).

[4] D. S. Elliott, and D. M. Barrett, "Mayo Clinic long-term analysis of the functional durability of the AMS 800 artificial urinary sphincter: a review of 323 cases," Journal of Urology, 159(4), 1206-8 (1998).

[5] C. A. Hajivassiliou, and I. G. Finlay, "Uneven pressure application by the artificial urinary sphincter: an explanation for tissue ischaemia?," British Journal of Urology Int., 83(4), 416-419 (1999).

[6] M. Hussain, Greenwell T. J., Venn S.N. et al., "The current role of the artificial urinary sphincter for the treatment of urinary incontinence," Journal of Urology, 174(2), 418-24 (2005).

[7] F. Maillet, J. M. Buzelin, O. Bouchot et al., "Management of artificial urinary sphincter dysfunction," European Urology, 46(2), 241-5 (2004).

[8] Y. Liu, H. Lv, X. Lan et al., "Review of electro-active shape-memory polymer composite," Composites Science and Technology, 69(13), 2064-2068 (2009).

[9] F. Carpi, and E. Smela, [Biomedical applications of electroactive polymer actuators] John Wiley & Sons, Ltd, (2009).

[10] C. Li, E. T. Thostenson, and T.-W. Chou, "Sensors and actuators based on carbon nanotubes and their composites: A review," Composites Science and Technology, 68(6), 1227-1249 (2008).

[11] L. Klouda, and A. G. Mikos, "Thermoresponsive hydrogels in biomedical applications," European Journal of Pharmaceutics and Biopharmaceutics, 68(1), 34-45 (2008).

[12] Q. Meng, and J. Hu, "A review of shape memory polymer composites and blends," Composites Part A: Applied Science and Manufacturing, 40(11), 1661-1672 (2009).

[13] C. Ohm, M. Brehmer, and R. Zentel, "Liquid crystalline elastomers as actuators and sensors," Advanced Materials, 22(31), 3366-3387 (2010).

[14] W. H. Jager, [Conjugated polymers as actuators for medical devices and microsystems] CRC Press, Taylor & Francis Group, 8 (2011).

[15] Y. Bar-Cohen, [Electroactive polymer (EAP) actuators as artificial muscles: Reality, potential, and challenges] SPIE Press, (2001).

[16] F. Carpi, D. De Rossi, R. Kornbuhl et al., [Dielectric elastomers as electromechanical transducers] Elsevier, (2008).

[17] G. Kofod, M. Paajanen, and S. Bauer, "New design concepts for dielectric elastomer actuators," Proc. SPIE, 6168, 61682J (2006).

[18] P. Lochmatter, [Development of a shell-like electroactive polymer (EAP) actuator] ETH Zürich, Zurich (2006).

[19] Q. Pei, M. A. Rosenthal, R. Pelrine et al., "Multifunctional electroelastomer roll actuators and their application for biomimetic walking robots," Proc. SPIE, 5051, 281 (2003).

[20] A. Wingert, M. D. Lichter, and S. Dubowsky, "On the design of large degree-of-freedom digital mechatronic devices based on bistable dielectric elastomer actuators," IEEE/ ASME Transactions on Mechatronics, 11(4), 448-456 (2006).

[21] Q. Pei, R. Pelrine, S. Stanford et al., "Electroelastomer rolls and their application for biomimetic walking robots," Synthetic Metals, 135-136, 129-131 (2003).

[22] R. Pelrine, R. D. Kornbluh, Q. Pei et al., "Dielectric elastomer artificial muscle actuators: Toward biomimetic motion," Proc. SPIE, 4695, 126 (2002).

[23] G. Kovacs, P. Lochmatter, and M. Wissler, "An arm wrestling robot driven by dielectric elastomer actuators," Smart Materials and Structures, 16, S306-S317 (2007).

[24] W.-P. Yang, and L.-W. Chen, "The tunable acoustic band gaps of two-dimensional phononic crystals with a dielectric elastomer cylindrical actuator," Smart Materials and Structures 17, 015011 (2008).

[25] R. Kornbluh and R. Pelrine, [High-performance acrylic and silicone elastomer] Elsevier, (2008).

[26] G. Kovacs, L. Düring, S. Michel et al., "Stacked dielectric elastomer actuator for tensile force transmission," Sensors and Actuators A, 155, 299-307 (2009).

[27] M. Benslimane and P. Gravesen, "Mechanical properties of dielectric elastomer actuators with smart metallic compliant electrodes," Proc. SPIE, 4695, 150 (2002).

[28] P. Dubois, S. Rosset, S. Koster et al., "Microactuators based on ion implanted dielectric electroactive polymer (EAP) membranes," Sensors and Actuators A: Physical 130-131, 147–154 (2006).

[29] C. Huang, Q. M. Zhang, G. deBotton et al., "All-organic dielectric-percolative three-component composite materials with high electromechanical response," Applied Physics Letters, 84(22), 4391-4393 (2004).

[30] T. Leippold, F. Marti, N. Blunschi et al., "The necessity of the second cuff in the AMS 800 double cuff system to provide satisfactory continence - study of a dynamic and static model," Journal of Urology, 175, 116 (2006).

[31] B. Müller, J. Ratia-Garcia, F. Marti et al., "Mechanical properties of urethral tissue," Journal of Biomechanics, 41, 61 (2008).

[32] H. Deyhle, [Elekrisch aktivierte Dünnfilmstrukturen aus Silikon] Master Thesis, Physics Department, ETH Zürich, Zurich (2007).

[33] R. Pelrine, R. Kornbluh, Q. Pei et al., "High-speed electrically actuated elastomers with strain greater than 100%," Science, 287, 836-839 (2000).

[34] H. Deyhle, M. Hirayama, F. Zuber et al., "Morphology of metal-coated silicone films," Eur. Cells. Mater., 16, 31 (2008).

[35] N. Bowden, S. Brittain, A. G. Evans et al., "Spontaneous formation of ordered structures in thin films of metals supported on an elastomeric polymer," Nature, 393, 146-149 (1998).

[36] M. Watanabe, "Striped-pattern formation of a thin gold film deposited onto a stretched elastic silicone substrate," Journal of Polymer Science: Part B: Polymer Physics, 43(12), 1532-1537 (2005).

[37] M. Y. Benslimane, H.-E. Kiil, and M. J. Tryson, "Dielectric electro-active polymer push actuators: performance and challenges," Polymer Int., 59, 415-421 (2010).

[38] W. Yuan, L. Hu, S. Ha et al., "Self-clearable carbon nanotube electrodes for improved performance of dielectric elastomer actuators," Proc. SPIE, 6927, 69270P (2008).

[39] M. O'Brien, S. Rosset, H. R. Shea et al., "Cutting the fat: artificial oscillators for lighter, cheaper, and slimmer devices," Proc. SPIE, 8340, this issue (2012).

[40] S. Rosset, P. Gebbers, B. M. O'Brien et al., "The need for speed," Proc. SPIE, 8340, this issue (2012).